A DATA WEIGHTING SCHEME FOR QUASISTATIC ULTRASOUND ELASTICITY IMAGING

L. Chen, R. J. Housden, G. M. Treece,
A. H. Gee and R. W. Prager

CUED/F-INFENG/TR 651

May 2010

University of Cambridge
Department of Engineering
Trumpington Street
Cambridge CB2 1PZ
United Kingdom

Email: lc420/rjh80/gmt11/ahg/rwp @eng.cam.ac.uk

A data weighting scheme for quasistatic ultrasound elasticity imaging

Lujie Chen, R. James Housden, Graham M. Treece,
Andrew H. Gee and Richard W. Prager

University of Cambridge
Department of Engineering
Trumpington Street
Cambridge CB2 1PZ

Abstract

The quality of quasistatic ultrasound strain images depends strongly on post-processing procedures (normalization, spatial and temporal filtering). Such procedures generally benefit from weighting the data to give more credence to high quality strain estimates. In this paper, we evaluate several different quality metrics on each post-processing procedure. The results suggest that no single weighting scheme works best for all procedures. Rather, $\mathrm{SNR_e}$ is well suited to normalization and a combined variance-based metric to temporal filtering. For spatial filtering, the various quality metrics produce similar results.

1 Introduction

In most ultrasonic elasticity imaging techniques, a displacement estimation method is used to measure the deformation of tissue. Strain data can be obtained by taking the gradient of the displacement field. As it is generally difficult to recover the underlying tissue elasticity, especially with the quasistatic approach [1], post-processed strain images are often displayed as the end product.

The post-processing strategy strongly affects the quality of such images. In early studies, multi-compression averaging was used to reduce noise [2]. More recently, composite images have been constructed from several strain fields using data quality metrics in weighting schemes [3, 4, 5]. The weights can be applied on a per-image [6, 3, 4] or per-pixel basis [5]. Although it may be subjective as to which approach produces the "best" images, it is clear that an effective data weighting scheme is important for strain image reconstruction.

The purpose of this study is to evaluate several quality metrics potentially suitable for weighting strain data. Developing a post-processing strategy introduced in a previous paper [5], we propose a novel weighting scheme that uses different metrics at different processing stages. Qualitative and quantitative comparisons of the various schemes are performed using simulated, *in vitro* and *in vivo* data.

2 Method

Three post-processing procedures are performed on the raw strain data (see [5] for details): normalization[1], followed by spatial filtering and then temporal filtering (persisting several strain fields). In each of these procedures, every strain datum is assigned a weight indicative of the estimation quality, so that unreliable strain estimates are given less credence than reliable ones. Whereas only one weighting scheme was considered in [5], here we evaluate the following six data quality metrics:

(1) **no weighting:** the same weight is assigned to all strain data.

[1]Normalization involves dividing the strain by an estimate of the local stress, to remove depth-dependent stress attenuation and other artefacts [6, 4, 5]. The stress field is estimated by assuming uniform stiffness and fitting a regression surface to the strain data.

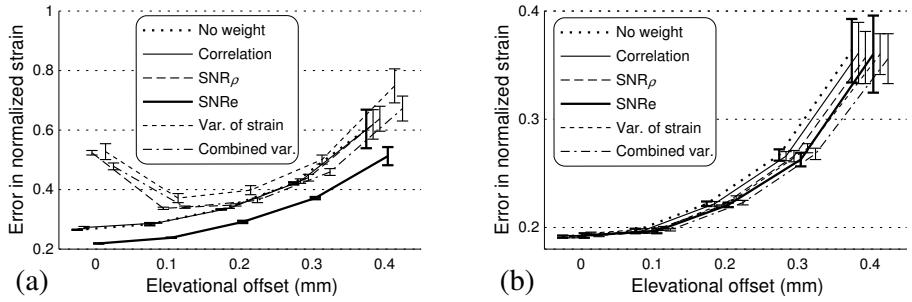

Figure 1: FEM simulation results of six quality metrics evaluated on the (a) normalization and (b) spatial filtering procedures.

(2) **correlation:** ρ, the post-alignment correlation coefficient between pre- and post-deformation windows (calculated using the envelope of the analytic RF signal).

(3) **SNR$_\rho$:** derived from correlation, originally given in [7] as $\rho/(1-\rho)$. We use a modified version to force SNR$_\rho$ to zero if $\rho \leq 2/3$, since a low ρ usually indicates a complete mismatch and an erroneous displacement estimate.

$$\mathrm{SNR}_\rho = \begin{cases} \frac{3\rho-2}{1-\rho} & \rho > \frac{2}{3} \\ 0 & \text{otherwise} \end{cases} \tag{1}$$

Note that, under reasonable assumptions, SNR$_\rho$ is inversely proportional to the phase gradient variance of matching windows [8].

(4) **SNR$_\mathbf{e}$** : defined as μ_s/σ_s, where μ_s and σ_s represent respectively the mean and standard deviation within a small region of supposedly uniform strain [9]. We use a 3×3 window region, since this is the smallest possible symmetric kernel.

(5) **the inverse of the variance of strain:** $1/\sigma_s^2$, again measured within a 3×3 window region, reflecting strain continuity.

(6) **combined variance:** $C_w = \sqrt{\mathrm{SNR}_\rho}/\sigma_s$, which combines intra- and inter-window precision estimates (SNR$_\rho$ and $1/\sigma_s^2$).

3 Results and discussion

3.1 Quantitative FEM simulations

Finite element modeling (FEM) was used to assess the effects of weighting on normalization and spatial filtering. The 3D displacement field of a block of tissue with uniform elasticity (10 kPa) was calculated using Abaqus 6.7 (Simulia, Rhode Island, USA). The probe displacement introduced an average strain of 1%. Pre- and post-deformation RF data was simulated using Field II [10] at elevational transducer offsets of 0, 0.1, 0.2, 0.3 and 0.4 mm (the out-of-plane displacement acts as a proxy for various real-world decorrelation effects). At each offset, strain images were calculated 100 times with different RF realizations. Image quality was judged using the average pixel-wise difference d between the post-processed strain and the ground truth (a uniform elasticity field of value 1).

Figure 1(a) shows the mean and ± 1 standard deviation of d across 100 trials evaluated on normalization alone. Irrespective of the elevational offset, the SNR$_\mathrm{e}$ weights produce the most accurate normalized strain field. The three variance-based weightings (SNR$_\rho$, $1/\sigma_s^2$ and C_w) exhibit interesting behaviour at 0 and 0.1 mm offset: the accuracy improves with signal decorrelation. To understand this seemingly irrational effect, consider the strain images and weights produced using SNR$_\rho$ and SNR$_\mathrm{e}$ in Figure 2 (the results with $1/\sigma_s^2$ and C_w are similar to those of SNR$_\rho$). In Figure 2(a), an implausibly bright (soft) region is produced in the upper half of the image. The

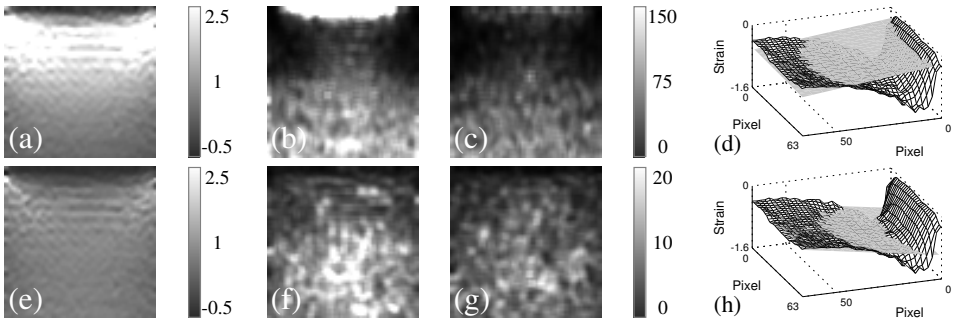

Figure 2: Normalized strain field based on (a) SNR_ρ and (e) SNR_e at zero elevational offset. SNR_ρ (b, c) and SNR_e (f, g) weights at 0 and 0.1 mm offset. Normalization surface based on (d) SNR_ρ and (h) SNR_e at zero offset. In (d) and (h), the meshed surface is the raw strain field before normalization.

SNR_ρ weights (Figure 2(b)) are high at the top of the frame because of the small deformation near the probe surface. These high weights bias the normalization surface towards the top (Figure 2(d)) and produce the artefactual bright region in Figure 2(a). At 0.1 mm elevational offset, the increased RF signal decorrelation reduces the SNR_ρ across the entire image, but disproportionally so at the top, since SNR_ρ is particularly sensitive to ρ when ρ is large (Equation (1)). Consequently, the normalization surface is less biased and the results are improved (Figure 1(a)). Unlike SNR_ρ, SNR_e (Figures 2(f) and (g)) is not regionally sensitive to signal decorrelation. The normalization surface (Figure 2(h)) fits closely to the main region of interest and the resulting post-processed strain image (Figure 2(e)) is more plausible for tissue of uniform stiffness.

Figure 1(b) shows the FEM results for the spatial filtering procedure (following normalization with SNR_e weights). The spatial filter spans $3 \times 3\,\mathrm{mm}^2$ and is weighted by Gaussian coefficients multiplied by the quality metric. The results indicate little difference between the various weighting schemes. This is most likely because the data quality does not vary dramatically within the $3 \times 3\,\mathrm{mm}^2$ kernel, so all the schemes effectively reduce to "no weighting".

3.2 *In vitro* phantom scan

The effect of weighting on temporal filtering was investigated using six consecutive strain fields from an elasticity phantom, as shown in Figures 3(a1-a6). Figures 3(a2) and (a3) suffer from regional and whole-frame displacement tracking errors, which are essentially unavoidable in practice. With no weighting, tracking errors are persisted in the strain images (Figures 3(b2-b6)). SNR_e offers little advantage (Figures 3(c2-c6)), since SNR_e weights strain data mildly and the distinction between high and low quality estimates is insufficient. The three variance-based weightings produce considerably better strain images (SNR_ρ: (d1-d6), $1/\sigma_s^2$: (e1-e6) and C_w: (f1-f6)).

A closer inspection of Figures 3(d3-d5), (e3-e5) and (f3-f5) reveals that C_w outperforms SNR_ρ and $1/\sigma_s^2$. The SNR_ρ weights fail to suppress a few small dark and bright patches in (d3-d5), because erroneous displacement estimates may occasionally attain similar SNR_ρ scores to accurate estimates. The $1/\sigma_s^2$ weights fail to suppress larger erroneous patches in (e3-e5). Although $1/\sigma_s^2$ can detect low quality at the boundaries of mismatched regions, it may be less effective inside such a region, since the strain estimates may be incorrect but nevertheless fairly continuous. C_w multiplies $\sqrt{\mathrm{SNR}_\rho}$ and $1/\sigma_s$, producing a high weighting only when both quantities are large. In essence, C_w provides a double check of strain quality by testing both the displacement estimation precision and the strain continuity.

Based on all the results, we propose a weighting scheme that applies SNR_e to normalization and C_w to spatial and temporal filtering.

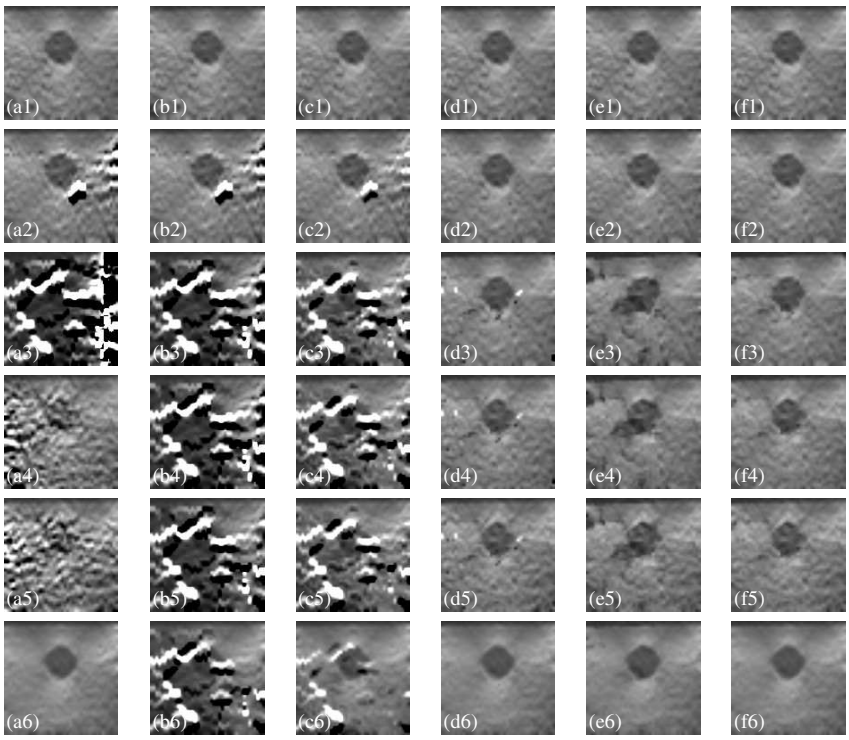

Figure 3: (a1-a6) Individual strain fields from the phantom scan. Strain images at each step of temporal filtering based on no weighting (b1-b6), SNR_e (c1-c6), SNR_ρ (d1-d6), $1/\sigma_s^2$ (e1-e6), and C_w (f1-f6). The ρ-based weights produce very similar results to (b1-b6). All strain images are normalized using SNR_e and no spatial filtering is applied. The grey scale is the same as that in Figure 2(a).

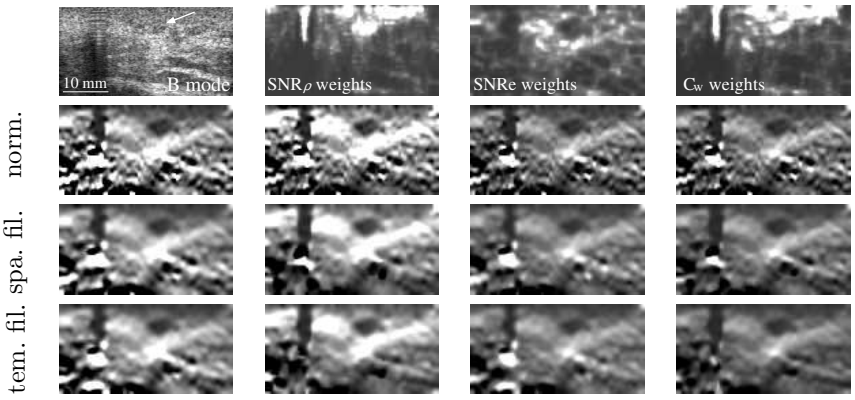

Figure 4: The first row shows the B-mode image of the neck nodule and the SNR_ρ, SNR_e and C_w weights. In the next three rows, each column shows strain images obtained using (a) no weighting, (b) SNR_ρ, (c) SNR_e and (d) the proposed scheme (SNR_e for normalization and C_w for spatial and temporal filtering); and each row indicates a post-processing procedure. Temporal filtering is applied to six consecutive strain fields. The grey scale is the same as that used in Figure 2(a).

3.3 *In vivo* scans

Four weighting schemes (no weighting, SNR_ρ, SNR_e and the proposed scheme), applied to all three post-processing stages, were tested on an *in vivo* scan of a neck nodule (Figure 4) and a testis (Figure 5). The nodule, indicated in the B-mode image, appears as a dark elliptical region in all strain images. The dark strip towards the left is caused by slight loss of contact between the transducer and the skin. RF signals in this region change very little before and after compression, resulting in high SNR_ρ and C_w, since there is high correlation and low variance. Conversely, the loss of contact induces low SNR_e due to near zero strain. Similar phenomena can be observed in the nodule region, where small deformations produce high SNR_ρ and C_w, but low SNR_e. The SNR_ρ weights are high towards the top of the frame, resulting in a biased normalization surface that is evident in Figure 4(b). The proposed scheme (Figure 4(d)) selects the most suitable quality metric at each stage (SNR_e for normalization and C_w for spatial and temporal filtering), producing a strain image with the fewest apparent artefacts.

The testis results (Figure 5) show a similar trend. The no weighting (a) and SNR_ρ (b) schemes do not produce a correctly normalized strain field. The SNR_e scheme (c) is less effective at suppressing artefacts around the testis than the proposed scheme (d).

4 Conclusions

We have demonstrated the importance of weighting schemes when post-processing strain images by normalization, spatial filtering and temporal filtering. FEM, *in vitro* and *in vivo* experiments all indicated that no single weighting scheme is ideally suited to each task. Rather, SNR_e is the preferred candidate for normalization, whereas the combined variance offers some advantages for temporal filtering. Spatial filtering is relatively insensitive to weighting, though we suggest the use of combined variance to avoid unnecessary computation when filtering in both time and space.

Acknowledgements

This work was funded by Translation Award 081511/Z/06/Z from the Wellcome Trust.

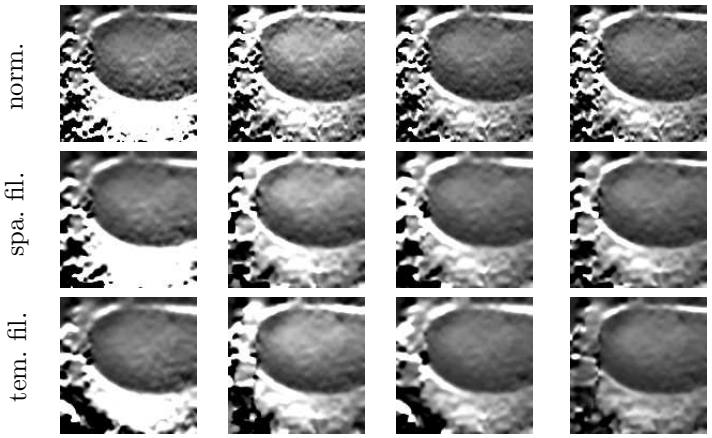

Figure 5: Results for the testis scan. Each column shows strain images obtained using (a) no weighting, (b) SNR$_\rho$, (c) SNR$_e$ and (d) the proposed scheme; and each row indicates a post-processing procedure. Temporal filtering is applied to six consecutive strain fields. The grey scale is the same as that used in Figure 2(a).

References

[1] J. Ophir, I. Céspedes, H. Ponnekanti, Y. Yazdi, and X. Li. Elastography: a quantitative method for imaging the elasticity of biological tissues. *Ultrasonic Imaging*, 13:111–134, 1991.

[2] T. Varghese, J. Ophir, and I. Cespedes. Noise reduction in elastograms using temporal stretching with multicompression averaging. *Ultrasound in Medicine and Biology*, 22(8):1043–1052, 1996.

[3] J. Jiang, T. J. Hall, and A. M. Sommer. A novel performance descriptor for ultrasonic strain imaging: a preliminary study. *IEEE Transactions on Ultrasonics, Ferroelectrics, and Frequency Control*, 53(6):1088–1102, 2006.

[4] J. Jiang, T. J. Hall, and A. M. Sommer. A novel image formation method for ultrasonic strain imaging. *Ultrasound in Medicine and Biology*, 33(4):643–652, 2007.

[5] J. E. Lindop, G. M. Treece, A. H. Gee, and R. W. Prager. An intelligent interface for freehand strain imaging. *Ultrasound in Medicine and Biology*, 34(7):1117–1128, 2008.

[6] K. M. Hiltawsky, M. Kruger, C. Starke, L. Heuser, H. Ermert, and A. Jensen. Freehand ultrasound elastography of breast lesions: clinical results. *Ultrasound in Medicine and Biology*, 27(11):1461–1469, 2001.

[7] I. Céspedes, J. Ophir, and S. K. Alam. The combined effect of signal decorrelation and random noise on the variance of time delay estimation. *IEEE Transactions on Ultrasonics, Ferroelectrics, and Frequency Control*, 44(1):220–225, 1997.

[8] G. M. Treece, J. E. Lindop, A. H. Gee, and R. W. Prager. Uniform precision ultrasound strain imaging. *IEEE Transactions on Ultrasonics, Ferroelectrics, and Frequency Control, in press*, 2009.

[9] I. Céspedes and J. Ophir. Reduction of image noise in elastography. *Ultrasonic Imaging*, 15(2):89–102, April 1993.

[10] J. A. Jensen. Field: A program for simulating ultrasound systems. In *Proceedings of the 10th Nordic-Baltic Conference on Biomedical Imaging*, pages 351–353, Tampere, 1996.